High-Level ab Initio and Density Functional Theory Evaluation of Combustion Reaction Energetics: NO_2 and HONO Elimination from Dimethylnitramine

Michael A. Johnson and Thanh N. Truong*

Henry Eyring Center for Theoretical Chemistry, Department of Chemistry, University of Utah, 315 S 1400 E, Room Dock, Salt Lake City, Utah 84112

Received: July 20, 1999

Dimethylnitramine (DMNA) is used as a model system for investigating accurate and efficient electronic structure methods for nitramines. Critical points on the potential energy surfaces of DMNA, CH_3NCH_3, CH_3NCH_2, NO_2, HONO, and the transition state to HONO elimination were located through geometry optimizations using the B1LYP, B3LYP, MPW1PW91, and BH&HLYP density functional methods, in addition to MP2, G2(MP2), and QCISD ab initio theories using the cc-pVDZ basis set. For cost-effective determination of nitramine reaction energetics, highly correlated single-point calculations at DFT geometries are recommended. Our best estimated reaction enthalpies for N−N bond scission and HONO elimination are 41.6 and −0.9 kcal/mol, respectively, determined at the QCISD(T)//QCISD level of theory. These numbers can be reproduced to within 1.3 kcal/mol for the N−N bond and to within 0.5 kcal/mol for the HONO reaction by calculating QCISD(T) energies at B1LYP geometries, thus saving considerable computational cost without sacrificing accuracy. Using the same strategy, the transition state energy for HONO elimination can be modeled to within 0.1 kcal/mol of the QCISD(T)//QCISD result.

1. Introduction

Accurate numerical models for combustion of high-energy (HE) materials have safety and educational benefits and are viable alternatives to dangerous experimental tests. Indeed, modeling an explosion is a challenging problem that requires extensive atomic-scale information such as detailed chemical reaction mechanisms with associated thermodynamic and kinetic parameters, many of which are still not known. Understanding the decomposition of HE molecules is a key element in the simulation of explosions and combustion of propellants.

The cyclic nitramines HMX ($(CH_2NNO_2)_4$) and RDX ($(CH_2NNO_2)_3$) are universal HE ingredients in the manufacture of propellants and explosives. Although HMX and RDX have unique decomposition pathways that may involve several hundred fundamental chemical reactions, NO_2 and HONO are believed to be common intermediates in their decomposition.[1−3] To illustrate this, Figure 1 shows a mechanism proposed by Zhao et al. for the unimolecular decomposition of RDX that is consistent with IRMPD experiments.[4] Symmetric triple dissociation was identified as the dominant primary reaction channel accounting for two-thirds of the decomposition. The remaining one-third undergoes N−N bond scission, and 77% of that one-third continues to decompose through HONO elimination; therefore, approximately one-fourth of RDX decomposition in these experiments proceeds via N−N bond scission followed by HONO elimination. Such information may be combined with the associated energetics and used directly as input data for combustion models[2] or used in conjunction with transition state theory to estimate reaction rate constants for use in future simulations.[5] In the absence of experimental data, thermodynamic and kinetic parameters must be calculated. Because of the large number of reactions involved, it is important to employ a methodology in building a database of reaction parameters that provides both efficiency *and* accuracy.

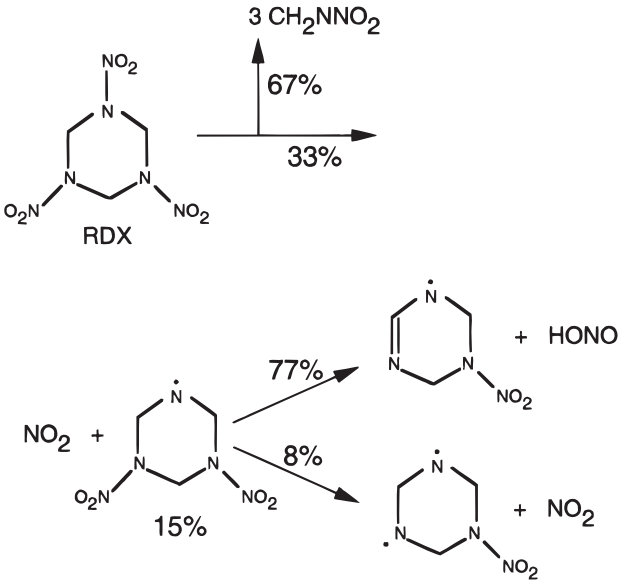

Figure 1. Initial steps in the unimolecular decomposition of RDX proposed on the basis of IRMPD experiments.

The main limitation of accurate ab initio molecular orbital (MO) methods is their cost, scaling as N^4 or greater, where N is the number of basis functions. Consequently, the use of large basis sets and high levels of correlation needed to generate accurate chemical kinetics data for many reactions involving large molecules is not presently feasible in the context of an ab initio MO methodology. Alternatively, density functional theory (DFT), with a formal scaling of N^3, provides cost-effective access to reasonably accurate ground-state chemical properties. However, current DFT methods do not perform as well in the

* Corresponding author.

10.1021/jp9925029 CCC: $18.00
Published on Web 10/15/1999

prediction of transition state properties as they do for calculating characteristics of equilibrium structures, and they generally underestimate reaction barriers.[6,7] Although several theoretical studies have focused on evaluating the various DFT functionals for use in nitramine studies, no one method has emerged as superior for consistently predicting efficient and accurate reaction energies, including transition state properties.[8,9]

The use of a strictly ab initio or strictly DFT methodology may not provide the optimal strategy for the study of large molecules such as nitramines. There is evidence in the literature that a single-point correlated calculation at the Hartree-Fock (HF) geometry gives acceptable results when the system under consideration is too large for optimization at a high level of theory. In particular, reasonable C−NO_2 barriers to rotation have been calculated using MP2 energy refinements at HF geometries.[10] Similar results were drawn from a study of rotational barriers in nitramines where DFT energies were calculated at HF geometries.[11] Although this technique has shown promise for the calculation of rotational barriers, it should be approached with caution when considering processes where chemical bonds are broken and/or formed. To give additional credibility to the practice of combining correlated methods with efficient geometry optimizations, the following fundamental questions should be addressed: (i) What level of theory is needed to capture accurate nitramine reaction energetics? (ii) What is the accuracy associated with calculating high-level ab initio corrections to energy at lower-level geometries? These are the questions that are addressed in this paper. By comparing the performance of efficient ab initio and DFT methods to one of the highest levels of theory that is currently available, namely, QCISD(T), we wish to establish a protocol for future studies on large HE molecules where high-level electronic structure calculations are not presently feasible.

Because of its smaller size and chemical similarity to the cyclic nitramines HMX and RDX, dimethylnitramine (DMNA, $(Me)_2NNO_2$) is often the first choice when selecting a model system for the study of HE nitramines.[12−17] In this study, we have systematically carried out DFT, MP2, G2(MP2), and QCISD calculations for the chemical properties of DMNA. Although it is believed that HONO elimination contributes not more than 10% to the overall decomposition of DMNA,[18] the importance of N−N bond homolysis and HONO elimination in this class of nitramines appears to be universal;[17−23] thus, we have focused our study on these two reactions.

2. Computational Details

All calculations for this study were carried out using the Gaussian 94 and Gaussian 98 quantum chemistry packages.[24,25] We performed full geometry optimizations for the following gas-phase species: DMNA, CH_3NCH_3, CH_3NCH_2, NO_2, HONO, and the transition state to HONO elimination. The transition state to NO_2 elimination from DMNA has been estimated to be either very shallow or not present;[18] therefore, it has not been considered in this work. The general approach for calculating reaction energies is that of taking differences in the total energy of the species listed above.

We have employed Dunning's correlation-consistent double-ζ basis set (cc-pVDZ): this basis set includes 2s and 1p polarization functions on hydrogen and 3s, 2p, and 1d polarization functions on carbon, nitrogen, and oxygen atomic centers and has been optimized for use in correlated calculations.[26] The density functionals used are Becke's one-[27] and three[28]-parameter hybrid functionals that include nonlocal correlation from the Lee−Yang−Parr[29,30] functional (B1LYP and B3LYP, respectively), the hybrid functional Becke-Half-and-Half-LYP[25] (BH&HLYP), and the one-parameter hybrid functional employing modified Perdew−Wang exchange and Perdew−Wang 91 correlation[31] (MPW1PW91). In addition to the density functional methods, we performed ab initio geometry optimizations using second-order Møller−Plesset perturbation theory (MP2) and quadratic configuration interaction with single and double substitutions (QCISD). To assess the significance of including triple substitutions in calculations for accurate energy, a triples contribution was added to the QCISD energy (QCISD(T)). As a double-check on the reliability of calculated reaction energies, we used the G2(MP2)[32] procedure. Briefly, this is a modified form of the original Gaussian-2 (G2) theory[33] that approaches high-level results through a series of calculations to determine appropriate corrections related to basis set size and correlation energy. The MP2 variety of G2 theory provides a computational savings over the original G2 formalism and is nearly as accurate, yielding calculated energies generally within ±3 kcal/mol of experimental values.[32] Additionally, we have included calculated reaction energies based on the recently proposed scaling-all-correlation (SAC) method.[34] SAC is a parametrized approach for extrapolation of electronic structure calculations to the limit of full valence electron correlation.

Harmonic frequencies were calculated for all molecules considered and at all levels of theory used, except QCISD, which demands excessive computational resources. A single imaginary frequency was confirmed at each theoretical level for the transition state to HONO elimination. Scaling of vibrational frequencies was not performed, except in the context of G2-(MP2) theory, where scaled HF frequencies are used to determine the zero-point energy. Otherwise, zero-point, thermal, and enthalpy corrections to electronic energy were taken from the standard results of Gaussian frequency calculations, and in the case of QCISD, these corrections were taken from the MP2 normal-mode analysis.

TABLE 1: Geometry (Å, degrees) of DMNA from Previous Studies

	6-31G*			6-31G**	6-311G**		
param	RHF[a]	MP2[a]	B3LYP[b]	BPW[c]	HF[d]	MP2[d]	exp[e]
N−N	1.344	1.387	1.384	1.409	1.349	1.396	1.382
N−O	1.197	1.240	1.232	1.243	1.190	1.227	1.223
N−C	1.454	1.457	1.458	1.462	1.456	1.459	1.460
<C−H>	1.081	1.091			1.081	1.092	1.121
O−N−O	125.2	126.1	126.0	126	125.2	126.2	130.4
O−N−N	117.4	116.9	117.0	117	117.4	116.9	114.8
C−N−C	120.2	118.4	120.3	119	119.3	116.6	127.6
C−N−N	115.8	113.8	115.5	115	115.7	113.3	116.2
<N−C−H>	109.7	109.5			109.7	110.0	101.9
C−N−N−O	165.1	161.1		164	164.0	159.3	
N−N−C−H	57.0	58.6			65.4	62.6	
α^f	29.1	38.1	30.3		31.1	41.3	0.0
β^g	1.3	2.4			1.8	3.1	

[a] From ref 37. [b] From ref 12. [c] From ref 37. [d] From ref 15. [e] Electron diffraction data from ref 41. [f] Angle between the C-N-C plane and N-N bond; see Figure 2. [g] Angle between the O-N-O plane and N-N bond; see Figure 2.

3. Results and Discussion

3.1. Geometry Comparison with Experiment. The geometry of DMNA has been examined in numerous studies, and a summary of the results is presented in Table 1. Emerging from these studies is the result that including polarization functions in the basis set is essential for describing pyramidalization about the amine nitrogen in DMNA (α; see Figure 2), and this result is applicable to other amines as well.[35−37] Although experimental

TABLE 2: Ground-State (Cs) Geometry (A, degrees) of DMNA from Various Methods Using the cc-pVDZ Basis Set (See Figure 2 for Atom and Angle Labels)

param	MPW1PW91	B1LYP	B3LYP	BH&HLYP	MP2	QCISD
N−N	1.371	1.384	1.387	1.357	1.400	1.402
N−O	1.218	1.225	1.227	1.208	1.230	1.221
N−C	1.448	1.458	1.457	1.448	1.461	1.466
C−H2	1.096	1.097	1.098	1.089	1.099	1.101
C−H3	1.103	1.105	1.106	1.096	1.107	1.108
C−H1	1.094	1.094	1.096	1.087	1.096	1.098
std dev	0.016	0.009	0.008	0.003	0.005	0.0
O−N−O	126.1	126.1	126.1	125.8	126.5	126.4
O−N−N	116.9	117.0	116.9	117.1	116.7	116.8
C−N−C	120.7	120.0	120.1	120.6	117.1	116.5
C−N−N	115.8	115.4	115.4	115.6	113.3	113.1
N−C−H2	107.5	107.4	107.5	107.3	107.0	106.9
N−C−H3	112.4	112.3	112.4	112.2	112.3	112.3
N−C−H1	109.6	109.7	109.6	109.9	109.7	109.8
std dev	2.1	1.7	1.8	2.0	0.3	0.0
C−N−N−O[a]	165.5	164.3	164.4	165.2	159.5	158.8
N−N−C−H3	52.6	53.9	53.1	55.4	58.9	59.2
α[b]	28.6	31.0	30.7	29.1	40.7	41.9
β[c]	1.5	1.6	1.7	1.3	2.4	2.5

[a] Angle is for *trans*-C−N−N−O. [b] Angle between the C−N−C plane and N−N bond. [c] Angle between the O−N−O plane and N−N bond.

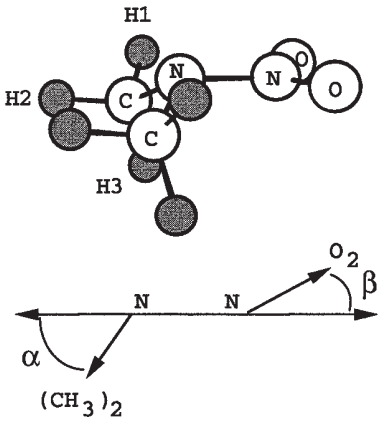

Figure 2. Geometry of DMNA (C_s symmetry) and the definitions of angles α and β.

gas-phase geometry from electron diffraction measurements indicate a planar (C_{2v}) arrangement, several studies have suggested that the theoretically predicted geometry for DMNA is likely to be more accurate than current experimental values.[12,15] It is noteworthy that a planar geometry of DMNA has been calculated in several studies where polarization functions were not included in the basis set.[13,16] Aside from the pyramidalization feature of DMNA, theoretical methods represented in Table 1 are generally in good agreement with experiment; thus, additional comparison to the experimental geometry is not necessary. Calculated geometry parameters (and total energies) for CH_3NCH_3, CH_3NCH_2, NO_2, and HONO are provided in the Supporting Information. As will be discussed shortly, geometry optimizations at the QCISD level of theory delivered the most accurate and reliable energetics of the methods tested. Thus, the QCISD geometry predictions are used as a standard against which to measure the performance of the other, less computationally demanding, theoretical methods.

3.2. Geometry Comparison with QCISD. Presented in Table 2 are the calculated geometry parameters of DMNA using the various DFT and ab initio methods employed in this work. Also included in the table are the numerical standard deviations from the QCISD/cc-pVDZ geometry produced by each method tested. When standard deviations are compared, it is possible to rank the computational methods on the basis of their ability to reproduce the QCISD geometry. This ranking brings forward several observations. To begin with, there is a good level of consistency in the ordering of methods based on standard deviations in both bond distances and angles. For example, the MP2 method models the QCISD equilibrium geometry of DMNA with the smallest standard deviation of 0.005 Å in bond distances and 0.3° in bond angles. MP2 also gave the best agreement in the degree of pyramidalization about the amine nitrogen; α = 40.7° in comparison to the QCISD value of 41.9°. On the other hand, the MPW1PW91 density functional yields the largest standard deviations from the QCISD geometry parameters; however, all of the standard deviations reported in Table 2 are quite small; thus, the methods reported there can be considered nearly equivalent on the basis of reproducing the QCISD equilibrium geometry.

Standard deviations from the QCISD/cc-pVDZ geometry of a smaller data set (three bond lengths and four bond angles) were calculated for the previously published geometries presented in Table 1 and compared to those determined in this work. In the context of this smaller data set, MP2/cc-pVDZ and MP2/6-311G**[15] were nearly identical in their ability to most accurately replicate the QCISD equilibrium geometry of DMNA over the other nine levels of theory considered. Of the DFT methods examined in our work and in previous studies, the B1LYP, B3LYP, and BPW[38] (see Table 1) functionals more closely modeled the QCISD geometry than did the BH&HLYP or the MPW1PW91 functionals. The HF/6-311G** and HF/6-31G* geometries reported in refs 15 and 37, respectively, were mediocre in their comparison to QCISD bond angles; however, they ranked behind all others in a comparison of bond lengths. The poor performance of the HF method in this context is likely not due to the basis sets used in those studies. For example, there is little difference in the geometry parameters calculated at the HF/6-31G* level and those calculated at the HF/6-311G** level (see Table 1). Similarly, in Table 1 there is a noticeable change in geometry between the HF/6-311G** and MP2/6-311G** methods. Therefore, the degree to which electron correlation is accounted for in the individual methods appears to be the most important factor for accurately modeling the equilibrium geometry of DMNA.

The transition state to HONO elimination from DMNA is believed to be the nearly planar five-membered ring configu-

TABLE 3: Bond Lengths (Å) in the Transition State to HONO Elimination from DMNA (See Figure 3 for Atom Labels)

param	6-31G*: B3LYP[a]	cc-pVDZ[b] MP2	BH&HLYP	MPW1PW91	B3LYP	B1LYP	QCISD
N2−O1	1.270	1.267	1.238	1.254	1.264	1.261	1.269
N2−O2	1.206	1.211	1.183	1.192	1.201	1.199	1.201
N−N	2.190	1.990	2.046	2.086	2.142	2.132	2.114
C1−N1	1.343	1.349	1.336	1.339	1.346	1.345	1.360
C2−N1	1.451	1.461	1.442	1.443	1.451	1.451	1.464
C1−H1	1.314	1.352	1.321	1.335	1.322	1.320	1.306
O1−H1	1.320	1.253	1.284	1.270	1.304	1.306	1.308
std dev	0.033	0.059	0.036	0.027	0.016	0.013	0.00

TABLE 4: Bond Angles (degrees) in the Transition State to HONO Elimination from DMNA (See Figure 3 for Atom Labels)

param	6-31G*: B3LYPa	cc-pVDZ[b] MP2	BH&HLYP	MPW1PW91	B3LYP	B1LYP	QCISD
O−N2−O	122.2	123.2	123.5	123.0	122.9	123.0	122.9
N1−N2−O1	101.6	105.1	103.9	102.7	102.2	102.5	103.3
N1−N2−O2	135.9	131.1	132.2	133.7	134.5	134.1	133.5
C1−N1−N2	94.6	97.6	96.8	96.4	95.5	95.6	95.1
C2−N1−N2	97.2	97.0	97.5	97.7	97.6	97.6	95.7
C−N1−C	117.1	115.4	117.8	117.2	117.2	117.3	115.6
O1−H1−C1	152.3	148.7	149.5	151.1	151.6	151.3	151.9
N1−C1−H1	97.0	94.5	95.1	94.9	96.0	96.0	96.1
N1−C1−H3	115.0	115.9	115.2	115.4	115.2	115.1	114.6
N1−C1−H2	119.7	120.2	119.2	120.0	119.9	119.7	119.0
std dev	1.31	1.91	1.51	1.17	1.04	0.99	0.00
C1−N−N−O1	6.5	8.7	8.4	8.5	7.8	7.8	7.3
C1−N−N−O2	180.1	180.0	178.7	179.7	179.7	179.5	179.3
γ[c]	29.6	25.8	29.4	27.5	28.7	29.1	31.3

[a] From ref 12; the values for N1−C1−H3 and N1−C1−H2 have been interchanged because of a suspected error in the original publication. [b] This work. [c] γ is the angle between the H2−C1−H3 plane and the C1−N1 bond vector.

TABLE 5: Reaction and Transition State (TS) Energies (kcal/mol) for N-N Bond Scission and HONO Elimination from DMNA

	N−N bond scission			HONO elimination: electronic[a]		ZPVE-corrected[b]		ΔH	
theory	ΔE[a]	ΔE[b]	ΔH_{298}	TS	ΔE	TS	ΔE	TS_{298}	ΔH_{298}
other methods	43.5[c]	43.8[d]	45.9[e]			45.2[f]	6.6[g]		
B1LYP	44.8	38.9	40.2	48.9	8.5	44.1	4.3	43.9	5.2
BH&HLYP	46.4	40.2	41.5	59.0	10.4	54.1	6.2	53.9	7.1
MPW1PW91	50.1	44.1	45.4	51.6	16.0	46.8	11.8	46.6	12.6
B3LYP	46.5	40.6	41.9	47.3	9.6	42.6	5.4	42.3	6.2
MP2	51.8	46.8	48.2	54.4	10.7	49.8	5.8	49.5	6.8
MP2-SAC	59.2	54.1	55.6	49.6	14.0	45.0	9.1	44.7	10.1
G2(MP2)	55.2	49.5	50.8	51.3	5.5	46.6	1.6	46.5	2.5
QCISD[h]	43.7	38.7	40.1	52.7	1.5	48.1	−3.4	47.8	−2.5
QCISD-SAC[h]	51.6	46.5	47.9	44.6	2.4	39.9	−2.4	39.7	−1.5
QCISD(T)//QCISD[h]	45.2	40.2	41.6	48.4	3.0	43.8	−1.9	43.5	−0.9
exp			43.3[i], 46.2[j]					≥38[k]	−1 to −3[j]

[a] Electronic energy only. [b] Electronic energy plus a zero-poing vibrational energy correction. [c] MC-SCF, from ref 14. [d] BPW density functional method reported in ref 38; other values from ref 12 include 41.1 (B3LYP/6-31G*) and 45.1 kcal/mol (MP2/6-31G*). [e] BAC-MP4 from ref 42. [f] B3LYP/6-31G*; also 53.8 kcal/mol (MP2/6-31G*) from ref 12. [g] B3LYP/6-31G* from ref 12. [h] Zero-point vibrational energy and thermal energy corrections are taken from MP2 vibrational frequencies. [i] From ref 43. [j] Estimate from ref 18. [k] Estimate from ref 18. Other estimates from ref 44 include 41 and 46 kcal/mol for analogous HONO eliminations from 2-nitropropane and nitroethane, respectively.

ration shown in Figure 3. The corresponding geometry parameters are presented in Tables 3 (bond lengths) and 4 (bond angles). Included also in these tables are results from Harris and Lammertsma, who have performed similar calculations at the B3LYP/6-31G* level of theory.[12] Again, ranking the standard deviations generated by each method relative to the QCISD geometry gives rise to remarkable consistencies in Tables 3 and 4. The B1LYP density functional approach provides the best model of the QCISD transition state geometry in both bond distances and bond angles, yielding standard deviations of 0.013 Å for the former and 0.99° for the latter. Previously we noted that MP2 reproduces the QCISD equilibrium geometry of DMNA rather well. Conversely, MP2 ranks behind all others tested in modeling the transition state geometry,

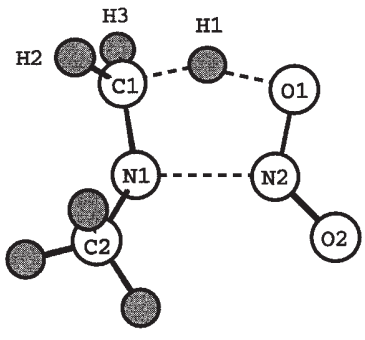

Figure 3. Geometry of the transition state to HONO elimination from DMNA.

TABLE 6: Comparison of Reaction Energies (kcal/mol) Calculated Using the Various Strategies Indicated

				HONO elimination					
	N−N bond scission			electronic[a]		ZPVE−corrected[b]		ΔH	
theory	ΔE^a	ΔE^b	ΔH_{298}	TS	ΔE	TS	ΔE	TS_{298}	ΔH_{298}
QCISD	43.7	38.7	40.1	52.7	1.5	48.1	−3.4	47.8	−2.5
QCISD//MP21	43.8	38.7	40.1	53.5	1.4	48.9	−3.5	48.6	−2.5
QCISD//B1LYP	43.5	37.5	38.8	52.5	1.3	47.7	−2.9	47.5	−2.1
QCISD(T)//QCISD	45.2	40.2	41.6	48.4	3.0	43.8	−1.9	43.5	−0.9
QCISD(T)//MP2	45.2	40.1	41.5	49.5	3.0	44.8	−1.9	44.6	−0.9
QCISD(T)//B1LYP	45.0	39.0	40.3	48.5	3.0	43.7	−1.3	43.5	−0.4
exp[c]			43.3, 46.2					≥38	−1 to −3

[a] Electronic energy only. [b] Electronic energy plus a zero-point vibrational energy correction. [c] See Table 5.

producing standard deviations from the QCISD values of 0.059 Å in bond lengths and 1.91° in bond angles.

To summarize the results of our geometry analysis, structural changes for DMNA are quite small between the six theoretical treatments considered. The B1LYP density functional gave the smallest overall standard deviation from the QCISD transition state geometry. Similarly, the MP2 method seems most likely to duplicate QCISD equilibrium geometries and least likely to model the QCISD transition state structure.

3.3. Energetics. Presented in Table 5 are the electronic and zero-point vibrational energy corrected reaction energies, in addition to the standard enthalpy of reaction for N−N bond scission and HONO elimination from DMNA. As a starting point for a discussion of energetics, Table 5 highlights the need for adding zero-point energy corrections to electronic energy for purposes of comparison to experimental values. Typically, the electronic and zero-point corrected reaction energies differ by about 5 kcal/mol for the reactions studied. Correcting to enthalpy at 298 K is less critical and accounts for only about 0.5 kcal/mol in the transition state and 1.0−1.5 kcal/mol in the equilibria state-to-state energies.

Shown in Figure 4 are graphical representations of the data presented in Table 5. An appropriate method for calculating reaction energetics cannot be determined by considering N−N bond breaking alone. To illustrate, panel a of Figure 4 depicts the data related to N−N bond homolysis. In comparison to all methods tested and the experimental numbers provided, the MP2, QCISD-SAC, and G2(MP2) methods appear to overestimate the N−N bond energy. The BH&HLYP, B3LYP, and B1LYP density functional methods are in reasonable agreement with the highest level of theory shown (QCISD). This result is similar to that reported in refs 9 and 8 regarding the performance of the BH&HLYP and B3LYP density functional methods, respectively. On the other hand, it appears that both DFT and MP2 methods are inadequate for calculating the energy associated with HONO elimination (see panel b of Figure 4). Shaw and Walker, on the basis of heats of formation, have estimated the reaction enthalpy for HONO elimination to be 1−3 kcal/mol exothermic under standard conditions.[18] Agreement with this estimation can be achieved only when electron correlation is accounted for at a high level of theory. Our calculated standard enthalpy of reaction for HONO elimination is −2.5 kcal/mol at the QCISD/cc-pVDZ level of theory, and this number increases to −0.9 kcal/mol when a correction is made for the approximate inclusion of triples (QCISD(T)//QCISD). It is worth noting that G2(MP2) theory predicts the reaction enthalpy for HONO elimination (2.5 kcal/mol) to a greater degree of accuracy than MP2 and the DFT methods considered, albeit still outside the range of −1 to −3 kcal/mol. For the general parametrization given in ref 34, the QCISD-SAC method performed well, giving a standard enthalpy of −1.5 kcal/mol for HONO elimination,

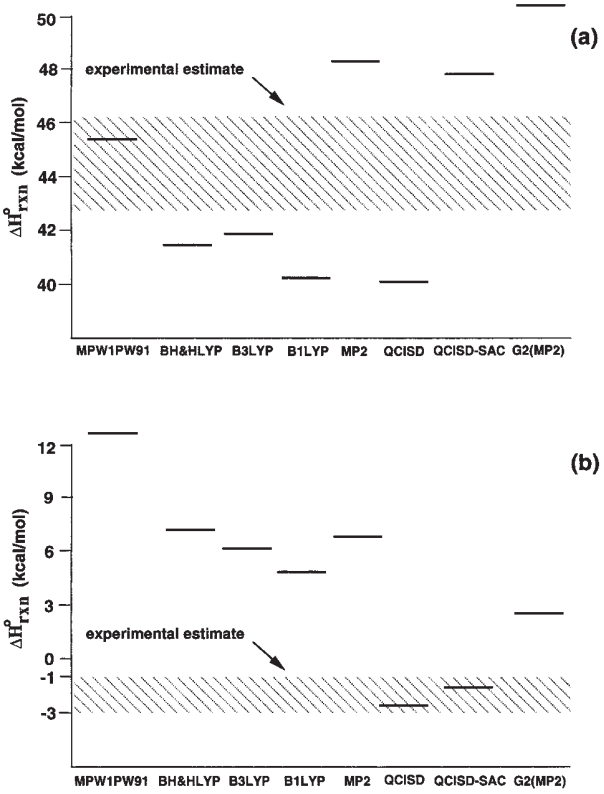

Figure 4. Graphical representation of the standard reaction enthalpy data presented in Table 5: (a) Enthalpy for N−N bond homolysis. (b) Standard enthalpy of reaction for HONO elimination.

but to achieve such accuracy, a single QCISD calculation is still necessary. On the other hand, the MP2-SAC method offers computational efficiency, but standard enthalpies are sharply overestimated at 55.6 kcal/mol for N−N bond breaking and 10.1 kcal/mol for HONO elimination. This may be improved by the use of reaction parameters specifically optimized for HE molecules.

Elimination of HONO from DMNA has not been directly observed by experiment; thus, the best available activation energy for this reaction is a lower-bound estimate of 38 kcal/mol.[18] This is of limited value in the present study because all of the methods tested are in accordance with this number. However, we can draw some insight from the transition state energies reported in Table 5. First, the overestimation of transition state energies by perturbation theory[39] and the similar performance of MP2 and the BH&HLYP functional in this regard[7] have been observed in other studies and appear to be general trends. The MP2 and BH&HLYP methods gave the highest enthalpies of activation at 298 K (TS_{298}) with 49.5 and 53.9 kcal/mol, respectively. As mentioned in the Introduction,

DFT often underestimates barrier heights, and the B3LYP method gave the lowest calculated barrier at 42.3 kcal/mol. In consideration of these boundaries, we believe the most reliable enthalpy barrier to HONO elimination at 298 K is 43.5 kcal/mol, resulting from our most accurate calculations, QCISD(T)//QCISD. This result again implies that a high level of theory is required to adequately describe nitramine reaction energetics. Further support for this is provided by previous studies that suggest the necessity of a multireference wavefunction for the study of similar reactions.[12,40]

Because of the computational cost, full geometry optimizations at the QCISD (or higher) level of theory are often not practical. To circumvent this, we next consider the possibility of performing energy refinements to stationary points on potential energy surfaces determined at lower levels of theory. The results of our geometry analysis (section 3.2) suggest that MP2 and B1LYP geometries are optimal for this purpose. Presented in Table 6 are reaction and transition state energies calculated as high-level energy refinements at MP2 and B1LYP geometries. As expected from the results of our geometry analysis, the QCISD(T)//MP2 approach reproduces QCISD(T)//QCISD energy changes between equilibrium states and the QCISD(T)//B1LYP method duplicates QCISD(T)//QCISD barrier heights, in both instances to within 0.1 kcal/mol. On the other hand, QCISD(T) energy refinements at MP2 structures for the transition state to HONO elimination differ by only about 1 kcal/mol from the complete QCISD(T)//QCISD treatment; this together with the fact that MP2 ranked behind all other methods considered for predicting the QCISD transition state geometry gives an estimate of the numerical uncertainty associated with performing accurate single-point calculations for energy at previously optimized geometries. It is also worth noting that, although the B1LYP functional ranked next to last in predicting the QCISD equilibrium bond lengths of DMNA, the difference in electronic energy between QCISD(T)//QCISD and QCISD(T)//B1LYP is only about 0.2 kcal/mol; the 1.3 kcal/mol difference in N−N bond enthalpy between these two approaches appears to be due to differences in the calculated harmonic frequencies.

In consideration of computational efficiency and the results presented here, geometry optimizations using DFT methods followed by energy refinements to QCISD or QCISD(T) levels are recommended for the efficient and accurate calculation of nitramine reaction energies. The variation in energy from full geometry optimization at the QCISD level is expected to be on the order of 1 or 2 kcal/mol for such an approach.

4. Conclusions

Our theoretical results suggest that a high level of theory, configuration interaction for example, is required to achieve satisfactory accuracy for nitramine reaction energetics. With the exception of QCISD (and QCISD-SAC), all methods considered predict reaction enthalpies for HONO elimination from DMNA that are outside the boundary of the experimental estimate. Differences in predicted geometries between the theoretical methods studied are all within an acceptable range, and the B1LYP density functional best reproduces the QCISD geometry at the transition state to HONO elimination. Calculating QCISD(T) energy refinements at B1LYP geometries models the QCISD(T)//QCISD enthalpy barrier to HONO elimination to within 0.1 kcal/mol and the enthalpy change for the same reaction to within 0.5 kcal/mol. The same technique reproduces the reaction enthalpy for N−N bond homolysis to within 1.3 kcal/mol of the QCISD(T)//QCISD value.

In addition to providing information related to the energetic properties of DMNA, the results presented here give support to the practice of combining high-level energy refinements with less expensive geometry optimizations. The proposed strategy shows promise for the study of energetic compounds such as HMX and RDX.

Acknowledgment. This research is supported by the University of Utah Center for the Simulation of Accidental Fires & Explosions, funded by the Department of Energy, Lawrence Livermore National Laboratory, under Subcontract B341493. We also gratefully acknowledge computational support from the University of Utah Center for High Performance Computing.

Supporting Information Available: Tables of experimental and calculated molecular geometries and total energies including zero-point vibrational energies and enthalpies for DMNA, *trans*-HONO, NO_2, and $(CH_3)_2N$ and CH_3NCH_2 radicals. This material is available free of charge via the Internet at http://pubs.acs.org.

References and Notes

(1) Yetter, R. A.; Dryer, F. L.; Allen, M. T.; Gatto, J. L. *J. Propul. Power* **1995**, *11*, 683.
(2) Davidson, J. E.; Beckstead, M. W. *J. Propul. Power* **1997**, *13*, 375.
(3) Behrens, R., Jr.; Bulusu, S. *J. Phys. Chem.* **1992**, *96*, 8877.
(4) Zhao, X.; Hintsa, E. J.; Lee, Y. T. *J. Chem. Phys.* **1988**, *88*, 801.
(5) Duncan, W. T.; Bell, R. L.; Truong, T. N. *J. Comput. Chem.* **1998**, *19*, 1039.
(6) Nguyen, M. T.; Creve, S.; Vanquickenborne, L. G. *J. Phys. Chem.* **1996**, *100*, 18422.
(7) Zhang, Q.; Bell, R.; Truong, T. N. *J. Phys. Chem.* **1995**, *99*, 592.
(8) Pai, S. V.; Chabalowski, C. F.; Rice, B. M. *J. Phys. Chem.* **1996**, *100*, 15368.
(9) Rice, B. M.; Pai, S. V.; Chabalowski, C. F. *J. Phys. Chem. A* **1998**, *102*, 6950.
(10) Head-Gordon, M.; Pople, J. A. *Chem. Phys. Lett.* **1990**, *173*, 585.
(11) Habibollahzadeh, D.; Murray, J. S.; Grice, M. E.; Politzer, P. *Int. J. Quantum Chem.* **1993**, *45*, 15.
(12) Harris, N. J.; Lammertsma, K. *J. Phys. Chem. A* **1997**, *101*, 1370.
(13) Politzer, P.; Sukumar, N.; Jayasuriya, K.; Ranganathan, S. *J. Am. Chem. Soc.* **1988**, *110*, 3425.
(14) Roszak, S. *THEOCHEM* **1994**, *304*, 269.
(15) Smith, G. D.; Bharadwaj, R. K.; Bedrov, D.; Ayyagari, C. *J. Phys. Chem. B* **1999**, *103*, 705.
(16) Sumpter, B. G.; Thompson, D. L. *J. Chem. Phys.* **1988**, *88*, 6889.
(17) McQuaid, M. J.; Miziolek, A. W.; Sausa, R. C.; Merrow, C. N. *J. Phys. Chem.* **1991**, *95*, 2713.
(18) Shaw, R.; Walker, F. E. *J. Phys. Chem.* **1977**, *81*, 2572.
(19) Capellos, C.; Papagiannakopoulos, P.; Liang, Y.-L. *Chem. Phys. Lett.* **1989**, *164*, 533.
(20) Adams, G. F.; Shaw, R. W. J. *Annu. Rev. Phys. Chem.* **1992**, *43*, 311.
(21) Zuckermann, H.; Greenblatt, G. D.; Haas, Y. *J. Phys. Chem.* **1987**, *91*, 5159.
(22) Botcher, T. R.; Wight, C. A. *J. Phys. Chem.* **1993**, *97*, 9149.
(23) Botcher, T. R.; Wight, C. A. *J. Phys. Chem.* **1994**, *98*, 5441.
(24) Frisch, M. J.; Trucks, G. W.; Schlegel, H. B.; Gill, P. M. W.; Johnson, B. G.; Robb, M. A.; Cheeseman, J. R.; Keith, T.; Petersson, G. A.; Montgomery, J. A.; Raghavachari, K.; Al-Laham, M. A.; Zakrzewski, V. G.; Ortiz, J. V.; Foresman, J. B.; Cioslowski, J.; Stefanov, B. B.; Nanayakkara, A.; Challacombe, M.; Peng, C. Y.; Ayala, P. Y.; Chen, W.; Wong, M. W.; Andres, J. L.; Replogle, E. S.; Gomperts, R.; Martin, R. L.; Fox, D. J.; Binkley, J. S.; Defrees, D. J.; Baker, J.; Stewart, J. P.; Head-Gordon, M.; Gonzalez, C.; Pople, J. A. *Gaussian 94*, Revision E.2; Gaussian, Inc.: Pittsburgh, PA, 1995.
(25) Frisch, M. J.; Trucks, G. W.; Schlegel, H. B.; Scuseria, G. E.; Robb, M. A.; Cheeseman, J. R.; Zakrzewski, V. G.; Montgomery, J. A., Jr.; Stratmann, R. E.; Burant, J. C.; Dapprich, S.; Millam, J. M.; Daniels, A. D.; Kudin, K. N.; Strain, M. C.; Farkas, O.; Tomasi, J.; Barone, V.; Cossi, M.; Cammi, R.; Mennucci, B.; Pomelli, C.; Adamo, C.; Clifford, S.; Ochterski, J.; Petersson, G. A.; Ayala, P. Y.; Cui, Q.; Morokuma, K.; Malick, D. K.; Rabuck, A. D.; Raghavachari, K.; Foresman, J. B.; Cioslowski, J.; Ortiz, J. V.; Stefanov, B. B.; Liu, G.; Liashenko, A.; Piskorz, P.; Komaromi, I.; Gomperts, R.; Martin, R. L.; Fox, D. J.; Keith, T.; Al-Laham, M. A.; Peng, C. Y.; Nanayakkara, A.; Gonzalez, C.; Challacombe, M.; Gill, P. M. W.; Johnson, B.; Chen, W.; Wong, M. W.; Andres, J. L.; Gonzalez, C.;

Head-Gordon, M.; Replogle, E. S.; Pople, J. A. *Gaussian 98*, Revision A.6; Gaussian, Inc.: Pittsburgh, PA, 1998.
(26) Dunning, T. H., Jr. *J. Chem. Phys.* **1989**, *90*, 1007.
(27) Becke, A. D. *J. Chem. Phys.* **1996**, *104*, 1040.
(28) Becke, A. D. *J. Chem. Phys.* **1993**, *98*, 5648.
(29) Lee, C.; Yang, W.; Parr, R. G. *Phys. Rev. B* **1988**, *37*, 785.
(30) Miehlich, B.; Savin, A.; Stoll, H.; Preuss, H. *Chem. Phys. Lett.* **1989**, *157*, 200.
(31) Adamo, C.; Barone, V. *Chem. Phys. Lett.* **1997**, *274*, 242.
(32) Curtiss, L. A.; Raghavachari, K.; Pople, J. A. *J. Chem. Phys.* **1993**, *98*, 1293.
(33) Curtiss, L. A.; Raghavachari, K.; Trucks, G. W.; Pople, J. A. *J. Chem. Phys.* **1991**, *94*, 7221.
(34) Fast, P. L.; Corchado, J.; Sanchez, M. L.; Truhlar, D. G. *J. Phys. Chem. A* **1999**, *103*, 3139.
(35) Boggs, J. E.; Niu, Z. *J. Comput. Chem.* **1985**, *6*, 46.
(36) Ritchie, J. P. *J. Am. Chem. Soc.* **1989**, *111*, 2517.
(37) Khaikin, L. S.; Grikina, O. E.; Vilkov, L. V.; Palafox, M. A.; Boggs, J. E. *J. Struct. Chem.* **1993**, *34*, 2.
(38) Politzer, P.; Lane, P.; Grice, M. E.; Concha, M. C.; Redfern, P. C. *THEOCHEM* **1995**, *338*, 249.
(39) Deng, L.; Branchadell, V.; Ziegler, T. *J. Am. Chem. Soc.* **1994**, *116*, 10645.
(40) Mowrey, R. C.; Page, M.; Adams, G. F.; Lengsfield, B. H., III. *J. Chem. Phys.* **1990**, *93*, 1857.
(41) Stølevik, R.; Rademacher, P. *Acta Chem. Scand.* **1969**, *23*, 672.
(42) Melius, C. F. *Chemistry and Physics of Energetic Materials*; Kluwer Academic Publishers: Dordrecht, The Netherlands, 1990.
(43) Lloyd, S. A.; Umstead, M. E.; Lin, M. C. *J. Energ. Mater.* **1985**, *3*, 187.
(44) Wodtke, A. M.; Hintsa, E. J.; Lee, Y. T. *J. Phys. Chem.* **1986**, *90*, 3549.